IOP Publishing

Dynamical Properties in Nanostructured and Low-Dimensional Materials

Michael G Cottam

Chapter 1

Introduction

In this chapter we will introduce many of the concepts that are central to the subject matter of this book. The topics will include a preliminary survey of the different waves or excitations in solids, along with a brief discussion of their linear and nonlinear (NL) dynamical properties, some examples of the low-dimensional structures and arrays that will be of importance for later applications and also the experimental and theoretical techniques that will be needed as tools in this study.

We will be less concerned here with the *static*, or time-independent, behaviour of solids and instead focus on the temporal (and usual spatial) evolution of some characteristic property that can propagate through a solid or be localized in certain regions. Corresponding to the latter case the *excitations* mentioned above can be considered as just the wave-like Fourier components of a general propagating signal in the solid. Physically the signal might, for example, consist of optical waves, vibrations of the atoms in the solid, the fluctuating magnetization in a magnetic material, or the collective motion of charges in a plasma. In a finite-sized solid the excitations will be required to satisfy boundary conditions at the surfaces or interfaces and so their properties may become modified. The novel properties of the excitations in certain finite structures, sometimes taken in conjunction with their NL dynamics as explained later, are of fundamental interest scientifically and may lead to a wide variety of practical device applications.

1.1 Types of excitations or waves

1.1.1 Fundamentals of excitations

We start by briefly describing the 'bulk' (or 'volume') excitations that are characteristic of effectively unbounded solids, where there are no surface effects to be taken into account. Details may be found in standard textbooks on solid-state physics (see, e.g., Kittel [1], Ashcroft and Mermin [2], and Grosso and Parravicini [3]). The modifying

doi:10.1088/978-0-7503-1054-3ch1

effects of surfaces and interfaces will be introduced next by following, for example, an approach based on symmetry arguments adopted for geometries of thin films and multilayers as in the book by Cottam and Tilley [4]. From a consideration of the symmetry and crystal lattices we shall arrive, via reciprocal lattices and Brillouin zones, at a form of Bloch's theorem for the elementary excitations.

A bulk crystalline solid may be regarded as a three-dimensional (3D) repetition in space of a *basis* or building block consisting of one or more atoms. The basis can be associated with the points on an infinitely extended lattice, which may be defined from symmetry in terms of three fundamental non-coplanar translational vectors, denoted by $\mathbf{a}_1$, $\mathbf{a}_2$ and $\mathbf{a}_3$. It then follows that the vector $\mathbf{R}$ connecting any two lattice points can be expressed as

$$\mathbf{R} = n_1\mathbf{a}_1 + n_2\mathbf{a}_2 + n_3\mathbf{a}_3, \tag{1.1}$$

where n_1, n_2 and n_3 take any integer values. Of course, the lattice may have other symmetry operations, such as rotations and reflections, that also leave the space lattice unchanged. We will see that the translations are particularly important and they imply that any physical quantity $f(\mathbf{r})$ at a general position $\mathbf{r}$ in the system satisfies

$$f(\mathbf{r}) = f(\mathbf{r} + \mathbf{R}) \tag{1.2}$$

for any $\mathbf{R}$ given by equation (1.1). Depending on the context, the quantity $f(\mathbf{r})$ might refer to a component of the magnetization vector or a charge density, for example.

The *unit cell* of a lattice is just the smallest volume with the property that all space can be filled by periodic repetitions of the unit cell for each lattice. Its specification is not unique, but one simple choice is the parallelepiped formed by the basic vectors $\mathbf{a}_1$, $\mathbf{a}_2$ and $\mathbf{a}_3$. Another construction is the *Wigner–Seitz* unit cell formed by drawing the perpendicular bisecting planes of the lattice vectors from any chosen lattice point to its neighbouring sites. Details are given in, e.g., [1–3]. Some choices of unit cell are shown in figure 1.1 for the special case of a two-dimensional (2D) oblique lattice with the basic vectors $\mathbf{a}_1$ and $\mathbf{a}_2$.

The next step is to introduce the *reciprocal lattice*. The basic vectors $\mathbf{b}_1$, $\mathbf{b}_2$ and $\mathbf{b}_3$ of this lattice in reciprocal space have the properties in 3D that

$$\mathbf{a}_i \cdot \mathbf{b}_j = 2\pi\delta_{ij}, \tag{1.3}$$

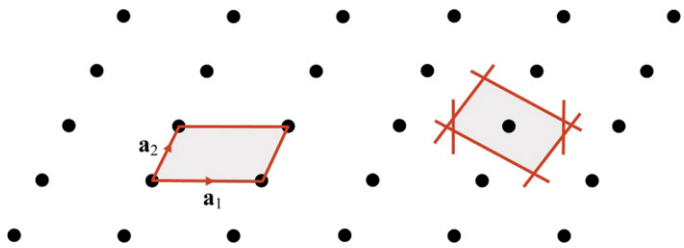

Figure 1.1. An oblique 2D space lattice with the basic vectors $\mathbf{a}_1$ and $\mathbf{a}_2$, showing two choices for the unit cell. The one on the left is a parallepiped and the Wigner–Seitz cell is illustrated on the right.

where i and j can take values 1, 2 or 3, and δ_{ij} is the Kronecker delta (equal to unity if the subscripts have the same value and zero otherwise). For example, we may write $\mathbf{b}_1 = (2\pi/V_0)(\mathbf{a}_2 \times \mathbf{a}_3)$ and so forth, with $V_0 = |\mathbf{a}_1 \cdot (\mathbf{a}_2 \times \mathbf{a}_3)|$ denoting the volume of the unit cell for the space lattice (see, e.g., [1]). Since $f(\mathbf{r})$ introduced in equation (1.2) is a periodic function (generally in 3D) it can be expressed in terms of a Fourier series using complex exponentials as

$$f(\mathbf{r}) = \sum_{\mathbf{Q}} F(\mathbf{Q}) \exp(i\mathbf{Q} \cdot \mathbf{r}), \tag{1.4}$$

where the $\mathbf{Q}$ vectors are required to satisfy $\exp(i\mathbf{Q} \cdot \mathbf{R}) = 1$. It is easily shown [1] that they are expressible in terms of the basic vectors of the reciprocal lattice as

$$\mathbf{Q} = \nu_1 \mathbf{b}_1 + \nu_2 \mathbf{b}_2 + \nu_3 \mathbf{b}_3, \tag{1.5}$$

with ν_1, ν_2 and ν_3 denoting integers. Finally we note that the unit cell of the reciprocal lattice is known as the *Brillouin zone*. The results are particularly straightforward in the case of a simple-cubic (sc) space lattice with lattice parameter a, because the reciprocal lattice is also sc. We may choose for the space lattice

$$\mathbf{a}_1 = a(1, 0, 0), \qquad \mathbf{a}_2 = a(0, 1, 0), \qquad \mathbf{a}_3 = a(0, 0, 1), \tag{1.6}$$

whereupon the basic vectors of the reciprocal lattice are simply

$$\mathbf{b}_1 = \frac{2\pi}{a}(1, 0, 0), \qquad \mathbf{b}_2 = \frac{2\pi}{a}(0, 1, 0), \qquad \mathbf{b}_3 = \frac{2\pi}{a}(0, 0, 1). \tag{1.7}$$

Now we discuss how the translational symmetries of the space and reciprocal lattices influence the elementary excitations in an unbounded solid. The most fundamental result is embodied in *Bloch's theorem* [5], which provides information about the spatial behaviour of the variable that describes the amplitude of the excitations. This variable, which we will denote generically as a function of position as $\psi(\mathbf{r})$, depends on the type of excitation. For example, it could be the quantum-mechanical wave function in the case of electronic states, an atomic displacement in the case of lattice vibrations (or phonons), or the fluctuating magnetization in the case of spin waves (SWs) (or magnons). These and other specific examples will be discussed in more depth in later chapters after we consider some general properties here. Bloch's theorem can be expressed generally as

$$\psi(\mathbf{r}) = \exp(i\mathbf{q} \cdot \mathbf{r}) U_{\mathbf{q}}(\mathbf{r}). \tag{1.8}$$

Here $U_{\mathbf{q}}(\mathbf{r})$ is a periodic amplitude function, just as in equation (1.2), and the phase factor $\exp(i\mathbf{q} \cdot \mathbf{r})$ describes a plane-wave variation of the amplitude $\psi(\mathbf{r})$. We shall not provide a proof of this result, since this can be found in the solid-state physics textbooks cited earlier. The wave vector $\mathbf{q}$ is evidently not unique, since it can be easily checked that values differing by any reciprocal lattice $\mathbf{Q}$ as defined in equation (1.5) will equally satisfy the requirements of Bloch's theorem. Typically, as we will see later, an energy eigenvalue E will be calculated for the dynamic variable $\psi(\mathbf{r})$ using its equation of

motion, e.g., in the case of an electronic excitation $\psi(\mathbf{r})$ could be the spatial wave function which satisfies Schrödinger's equation. On writing $E = \hbar\omega(\mathbf{q})$ with $\omega(\mathbf{q})$ representing the angular frequency of the excitation, it follows that we must have

$$\omega(\mathbf{q} + \mathbf{Q}) = \omega(\mathbf{q}). \tag{1.9}$$

In the idealized case of an unbounded crystal lattice the components of the vector $\mathbf{q}$ can take any real values, but equation (1.9) tells us that it is sufficient to take only $\mathbf{q}$ values that lie within the first Brillouin zone (the Wigner–Seitz cell centred at $\mathbf{q} = 0$). For the example of an sc space lattice mentioned earlier this gives $\mathbf{q} = (q_x, q_y, q_z)$ with

$$-\pi/a < q_x \leqslant \pi/a, \qquad -\pi/a < q_z \leqslant \pi/a, \qquad -\pi/a < q_z \leqslant \pi/a. \tag{1.10}$$

There are analogous results to equations (1.6), (1.7) and (1.10) for other 3D space lattices [1], such as body-centred cubic (bcc) and face-centred cubic (fcc) lattices.

While there are many 3D space lattices, there are relatively few in 2D. In fact, there are only five instead of fourteen. As we will see later, these 2D lattices will be important for thin films where there is translational symmetry in the 2D planes of atoms parallel to the surfaces, but not in the other dimension perpendicular to the surfaces. Consequently Bloch's theorem will be modified, as we discuss later. A 2D example, which is currently of considerable interest, is provided by *graphene*, which can be produced in the form of single sheets of atoms arranged in a 2D hexagonal or honeycomb space lattice (see, e.g., [6, 7]). The lattice structure is illustrated in figure 1.2 and it can be described in terms of two vectors $\mathbf{a}_1$ and $\mathbf{a}_2$ that form the basis of a unit cell with two carbon atoms per cell. There are two sublattices of carbon atoms, labelled A and B, as shown. Relative to the x- and y-coordinate axes we may write

$$\mathbf{a}_1 = \frac{\sqrt{3}\,a_0}{2}\left(\sqrt{3}, -1\right), \qquad \mathbf{a}_2 = \frac{\sqrt{3}\,a_0}{2}\left(\sqrt{3}, 1\right), \tag{1.11}$$

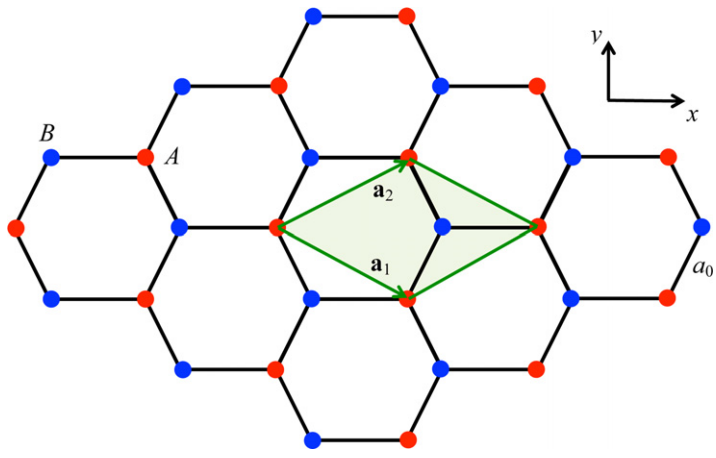

Figure 1.2. The spatial structure of a single sheet of graphene. Each carbon atom lies on one of two interpenetrating sublattices labelled A and B (shown here as red and blue circles, respectively). A possible choice for the two basic lattice vectors $\mathbf{a}_1$ and $\mathbf{a}_2$ is indicated, together with the corresponding unit cell (shown shaded).

where a_0 denotes the nearest-neighbour carbon–carbon distance. Also the basic vectors of the reciprocal lattice are simply [7]

$$\mathbf{b}_1 = \frac{2\pi}{3a_0}\left(1, -\sqrt{3}\right), \qquad \mathbf{b}_2 = \frac{2\pi}{3a_0}\left(1, \sqrt{3}\right). \tag{1.12}$$

In some other nanosystems to be considered later we might have just one direction in which there is a translational symmetry. For example, long nanowires and nanotubes that have a uniform, finite cross-sectional shape will exhibit translational symmetry with respect to their length coordinate only. Also one-dimensional (1D) linear-chain materials (such as the ferromagnetic chain pyroxene $NaCrGe_2O_6$ [8]) will have this property. By contrast, nanostructures that are finite in all three spatial dimensions will display no translational symmetry and are sometimes referred to as being zero-dimensional (0D).

1.1.2 Linear and nonlinear dynamics for excitations

Before looking further into the influence of the geometric structure on the excitations, it is useful to briefly consider how the excitations relate to the linear and NL aspects of the system dynamics. Although real physical systems might exhibit linear dynamics to a good approximation in many circumstances, it is nevertheless the case that NL behaviour will occur to some extent and may be enhanced under particular circumstances. It is to be expected that the excitations associated with the linear regime will consequently have their properties modified when nonlinearities are taken into account. It is important to enquire in what ways and to what degree this takes place and if there are practical effects to be utilized. Apart from this, we will find that there are some excitations associated with the NL regime of behaviour that have no counterpart in the linear approximation.

At this preliminary stage we will highlight some distinctions between the linear and NL dynamics of excitations, mainly by taking a few specific examples. These and other cases will then be explored in much more detail later, especially in chapter 7. Some general references covering NL dynamical phenomena, mostly for bulk properties, are the books by Yariv [9], Butcher and Cotter [10] and Mills [11] for NL optical materials and by Gurevich and Melkov [12] and Stancil and Prabakhar [13] for NL magnetic materials.

We start by considering an example of optical (electromagnetic) waves in a dielectric material, ignoring for the moment any specifically magnetic effects. The material is assumed to be homogeneous and sufficiently large that we need not explicitly take account of boundary effects. The response of the material to an external position- and time-dependent electric field $\mathbf{E}(\mathbf{r}, t)$ is conventionally described in terms of a dielectric function ε by writing

$$\mathbf{D}(\mathbf{r}, t) = \varepsilon_0 \int\int \varepsilon(\mathbf{r} - \mathbf{r}', t - t')\mathbf{E}(\mathbf{r}', t')\mathrm{d}^3\mathbf{r}'\mathrm{d}t'. \tag{1.13}$$

Here ε_0 is the permittivity of free space and $\mathbf{D}(\mathbf{r}, t)$ is the electric displacement (see, e.g., [14, 15]). The $\mathbf{D}$ and $\mathbf{E}$ vectors are also related to the polarization $\mathbf{P}$ in the material by

$$\mathbf{D}(\mathbf{r}, t) = \varepsilon_0\mathbf{E}(\mathbf{r}, t) + \mathbf{P}(\mathbf{r}, t), \tag{1.14}$$

where $\mathbf{P}(\mathbf{r}, t)$ is the polarization induced in the material. Rather than considering these quantities in terms of position and time, it is more useful for the dynamics to make Fourier transforms to a wave vector $\mathbf{q}$ and angular frequency ω according to, for example,

$$\mathbf{E}(\mathbf{r}, t) = \int\int \mathbf{E}(\mathbf{q}, \omega)\exp(\mathrm{i}\mathbf{q}\cdot\mathbf{r} - \mathrm{i}\omega t)\mathrm{d}^3\mathbf{q}\ \mathrm{d}\omega. \tag{1.15}$$

Then equation (1.13) can be re-expressed more compactly and conveniently as

$$\mathbf{D}(\mathbf{q}, \omega) = \varepsilon_0\varepsilon(\mathbf{q}, \omega)\mathbf{E}(\mathbf{q}, \omega), \tag{1.16}$$

while the corresponding result for the polarization is

$$\mathbf{P}(\mathbf{q}, \omega) = \varepsilon_0[\varepsilon(\mathbf{q}, \omega) - 1]\mathbf{E}(\mathbf{q}, \omega). \tag{1.17}$$

The $\mathbf{q}$-dependence of the dielectric function in the above two equations is known as *spatial dispersion* and arises from the fact that the dielectric term in equation (1.13) depends on the spatial separation $\mathbf{r} - \mathbf{r}'$ rather than on $\mathbf{r}$ and $\mathbf{r}'$ separately. However, in many cases this spatial dispersion may vanish or be negligible and we have simply a frequency-dependent dielectric function $\varepsilon(\omega)$ that is characteristic of the dynamical processes in the material being considered. Examples will be given later.

Before going any further we need to elaborate on two points regarding the above discussion. The first is that, in general, the vectors $\mathbf{D}$ and $\mathbf{P}$ may not necessarily be collinear with $\mathbf{E}$. The above relationships are still applicable provided the scalar dielectric function, $\varepsilon(\mathbf{q}, \omega)$ or $\varepsilon(\omega)$ as appropriate, is replaced by a second-rank tensor or equivalently a matrix in these cases. The second and more significant point is that for small values of the electric field there is a *linear* relationship, as expressed by equation (1.16), between $\mathbf{D}$ and $\mathbf{E}$. In other words, $\varepsilon(\mathbf{q}, \omega)$ is a constant function that does not depend on $\mathbf{E}$ and it is called the *linear dielectric function*. At larger electric-field values there is usually a *NL regime* in which the dielectric function becomes dependent on $\mathbf{E}$. A conventional approach in NL optics is to expand the dielectric function as a power series in terms of components of the electric-field components, as we describe in a later chapter. Various different NL effects can then be identified depending on which terms in the expansion are important. For example, the *Kerr-type nonlinearity* involves an effective NL dielectric function [10, 11] of the form

$$\varepsilon^{\mathrm{NL}} = \varepsilon + \rho\,|\mathbf{E}|^2. \tag{1.18}$$

Here both the linear part ϵ and the coefficient ρ before the field-dependent term may, in general, be functions of wave vector $\mathbf{q}$ and frequency ω.

To probe further some distinctions between the linear and NL dynamics arising due to the form of the dielectric function, we now turn to the basic equation satisfied by the electric field. This is just the electromagnetic wave equation arising from Maxwell's equations [14, 15]:

$$\varepsilon(\omega)\frac{\partial^2\mathbf{E}}{\partial t^2} - c^2\nabla^2\mathbf{E} = 0. \tag{1.19}$$

This result is the form appropriate for a transverse wave (i.e., when the wave vector **q** specifying the propagation direction is perpendicular to **E**) and c is the velocity of light in a vacuum. We note that the solution of this equation in the linear regime is relatively straightforward, because the linear dielectric function does not depend on **E** and so equation (1.19) is a linear differential equation. We are ignoring spatial dispersion here. The solution in this case where we assume an unbounded medium can be found in a plane-wave $\exp[i(\mathbf{q}\cdot\mathbf{r}-\omega t)]$ form, yielding

$$q^2 = \varepsilon(\omega)\omega^2/c^2. \tag{1.20}$$

This is just the implicit dispersion relation (ω versus q relationship) arising when the electromagnetic wave is coupled to the polarization field of the medium. The excitation is generally referred to as a *polariton*. If the dielectric function is just a constant and written as n^2, where n is the refractive index of the medium, we recover the usual dispersion relation $\omega = (c/n)q$ for a photon (light) with speed c/n in the medium. By contrast, a simple example of a frequency-dependent dielectric function occurs for an electron plasma, as for the gas of electrons in a metal or semiconductor in the presence of positive ions that ensure the overall charge neutrality. The plasma oscillations [1, 2] of the electron gas are known to define a characteristic angular frequency, the plasma frequency ω_p, given by ${\omega_p}^2 = n_0e^2/\varepsilon_0 m$ where n_0 is the 3D concentration of electrons, each having mass m and charge $-e$. It can be shown (see also chapter 4) that

$$\varepsilon(\omega) = \varepsilon_\infty\left(1 - \frac{{\omega_p}^2}{\omega^2}\right), \tag{1.21}$$

where ε_∞ is the limiting dielectric constant at frequencies well above ω_p and damping has been neglected. Substituting this into the expression in equation (1.20) and rearranging gives the plasmon-polariton dispersion relation explicitly as

$$\omega = \sqrt{{\omega_p}^2 + c^2q^2}\,. \tag{1.22}$$

This simple dispersion relation is drawn as the solid line in figure 1.3. We have also included for comparison the dashed line $\omega = cq$ which corresponds to the light line for propagation in a vacuum. There are two limiting regions of interest for the polariton. One is for $cq/\omega_p \ll 1$ when $\omega \simeq \omega_p$ and the other is for $cq/\omega_p \gg 1$ when $\omega \simeq cq$. There is also a band gap of forbidden frequencies where no plasmon-polaritons exist and this occurs here in the frequency range from 0 to ω_p.

The above discussion relates to an example of a *bulk* (or *volume*) excitation, since no account has been taken of any surface or boundary and the linear excitation propagates (or is wave-like) in all three spatial dimensions. Other linear types of polaritons may occur that are associated with surfaces and interfaces, and this behaviour will be one of the main topics in chapter 5.

We discussed earlier how NL effects could arise, for example, through a Kerr-type form of the dielectric function, as in equation (1.18). Before concluding this section we will outline a case of a NL polariton due to this term; more details will be given in chapter 7 (but see also [4]). This example is related to the phenomenon

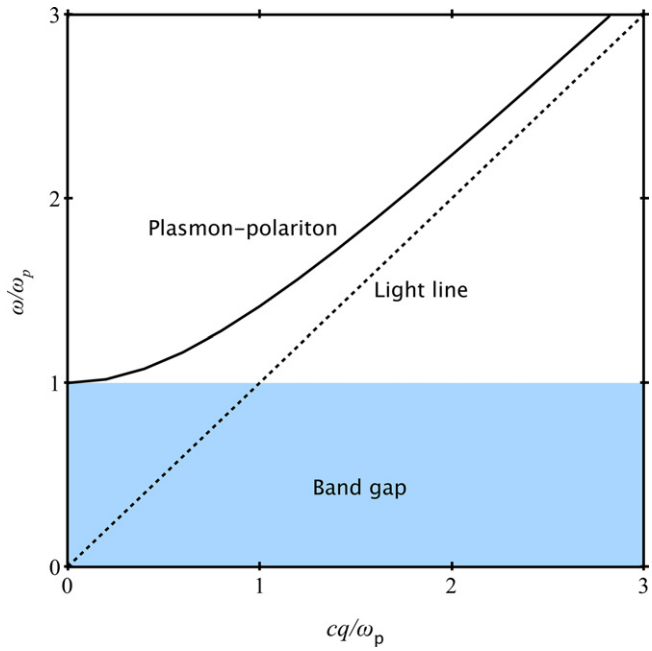

Figure 1.3. Dispersion relation for a linear plasmon-polariton (solid line) in a 3D material, as given by equation (1.22). The angular frequency, in terms of dimensionless ω/ω_p is plotted versus dimensionless wavenumber, in terms of cq/ω_p.

known as *self-guiding* and can occur for polaritons at an interface (see [16, 17] for reviews). We start with a qualitative description by recalling that within linear optics the guiding condition for a light wave to remain localized (through multiple internal reflections) within a film is that the refractive index of the film should exceed the refractive index of the bounding medium on each side [14, 15]. It might therefore be expected that, provided (i) ε and ρ in equation (1.18) are both positive and (ii) the electric-field term $|\mathbf{E}|^2$ can be localized with a large value near a surface, the situation will be broadly analogous to a guiding film with a large refractive index. The above conditions can, in fact, be realized as we now demonstrate by considering an interface between a linear medium and a Kerr NL medium.

Specifically we will assume that the NL medium fills the lower half-space $z < 0$, while a linear medium occupies the upper half-space $z > 0$. The interface between them corresponds to the plane $z = 0$ and the system is assumed to be infinite in the x- and y-coordinate directions. We look for solutions for which the electric field is a s-polarized wave, which means that it can be written as $\mathbf{E} = (0, E, 0)$ with its propagation being along the x-direction. From Bloch's theorem and assuming an angular frequency ω it follows that all electromagnetic-field quantities are proportional to $\exp(\mathrm{i}q_x x - \mathrm{i}\omega t)$. Substitution of equation (1.18) into the wave equation (1.19) yields

$$\frac{\mathrm{d}^2 E}{\mathrm{d}z^2} - \left(\kappa^2 - \rho\frac{\omega^2}{c^2}E^2\right)E = 0, \tag{1.23}$$

where we define κ, which is real for large enough q_x, by

$$\kappa^2 = {q_x}^2 - \varepsilon\omega^2/c^2 \tag{1.24}$$

and we assume solutions exist where E is real. The NL differential equation can then be solved by multiplying each side of (1.23) by $\mathrm{d}E/\mathrm{d}z$ and integrating to obtain

$$\left(\frac{\mathrm{d}E}{\mathrm{d}z}\right)^2 - \kappa^2 E^2 + \rho\frac{\omega^2}{2c^2}E^4 = 0. \tag{1.25}$$

Here a constant of integration has been set to zero on the assumption that both E and $\mathrm{d}E/\mathrm{d}z$ tend to zero as $z \to -\infty$ inside the NL medium. Next, equation (1.25) can be rearranged as an expression for $\mathrm{d}E/\mathrm{d}z$ as a function of z and directly integrated, giving

$$E = \frac{2^{1/2}c\kappa}{\rho^{1/2}\omega\cosh[\kappa(z + z_0)]} \tag{1.26}$$

as the solution appropriate for $z < 0$, where z_0 is another constant of integration. For completeness we also need to consider the solution for E in the linear medium (labelled 1) for $z > 0$. By contrast with equation (1.23) we now have a much simpler second-order linear differential equation, for which the solution satisfying the requirement $E \to 0$ as $z \to \infty$ is

$$E = E_1\exp(-\kappa_1 z). \tag{1.27}$$

Here $\kappa_1 = ({q_x}^2 - \varepsilon_1\omega^2/c^2)^{1/2}$ by analogy with equation (1.24), with ε_1 denoting the dielectric constant of medium 1 and as before we take κ_1 to be real. The constant E_1 is easily found from the electromagnetic boundary condition at the interface $z = 0$ that the tangential electric-field components must be continuous. We are still left, however, with the problem of finding the other constant z_0.

This kind of situation is typical of many problems involving NL excitations and in the present case it can be handled by finding another equation involving z_0 from consideration of the power flow in the propagating wave. In electromagnetism this comes from the time-averaged Poynting vector [14, 15] and further discussion will be deferred to chapter 7. However, we have demonstrated here by the form of equation (1.26) that a spatially localized electromagnetic wave can occur due to the non-linearity of the medium.

1.2 Survey of types of nanostructures

In the examples given so far, we have considered excitations in unbounded (bulk) media, in a 2D sheet (for graphene), or at the planar interface between two media. More generally there may be multiple boundaries (surfaces or interfaces) that affect the dimensionality and symmetries of the system, thus modifying the form of Bloch's theorem. Also, the boundaries introduce different length scales and here we will be mainly interested in effects in the range of nanometres (nm) up to micrometres (μm). We will now describe briefly some of the different nanostructures that will be considered in the following chapters. Examples are represented schematically in figure 1.4.

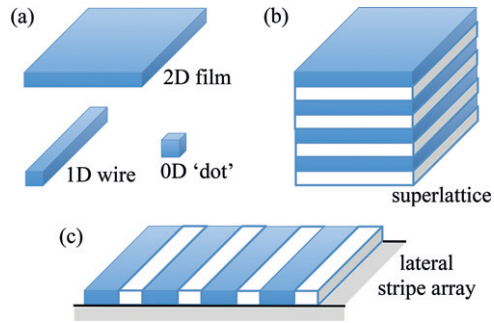

Figure 1.4. Schematic illustration of some types of nanostructures: (a) low-dimensional structures, (b) periodic multilayers or superlattices and (c) laterally patterned periodic structures.

1.2.1 Low-dimensional structures

In this category we have materials with reduced dimensionality as expressed in terms of the number of spatial dimensions in which there is translational symmetry. They include the 2D cases of thin films with finite thickness L and parallel planar surfaces, as well as sheets of atoms such as the graphene example mentioned earlier. They are characterized by a 2D space lattice associated with the planes of atoms parallel to the surfaces, as mentioned in subsection 1.1.1, and the form of Bloch's theorem will be modified slightly compared with equation (1.8) to become

$$\psi(\mathbf{r}_{\|}, z) = \exp\left(\mathrm{i}\mathbf{q}_{\|} \cdot \mathbf{r}_{\|}\right) U_{\mathbf{q}_{\|}}(\mathbf{r}_{\|}, z). \tag{1.28}$$

We have assumed that the z-axis is chosen to be perpendicular to the surfaces, so the in-plane vectors are $\mathbf{r}_{\|} = (x, y)$ and $\mathbf{q}_{\|} = (q_x, q_y)$. The challenge in solving for the excitations in films is finding the z-dependence of the amplitude term $U_{\mathbf{q}_{\|}}(\mathbf{r}_{\|}, z)$.

In the case of linear excitations in films we will often find later that this z-dependence is expressible as a linear combination of terms having the form $\exp(\mathrm{i}q_z^{(j)}z)$, where $q_z^{(j)}$ may be *complex* with a series of allowed values labelled by j (see, e.g., [4]). There are two possible situations that may arise. One is that $q_z^{(j)}$ is real and thus it represents the third wave-vector component of a bulk excitation in the film with total wave vector $\mathbf{q} = (\mathbf{q}_{\|}, q_z^{(j)})$. This bulk excitation is affected by the film surfaces because it must satisfy boundary conditions there. The other possibility is that $q_z^{(j)}$ may have an imaginary part, which we denote as $\mathrm{i}\kappa$. Then the $\exp(\mathrm{i}q_z^{(j)}z)$ term will involve a real factor such as $\exp(-\kappa z)$, which is characteristic of a localized surface excitation that decays with distance from one of the film surfaces. A surface excitation can therefore be typically described in terms of a 2D wave vector along with a decay length that is equal to κ^{-1}.

The category of low-dimensional structures also includes nanowires (or nanorods), which have just one direction of translational symmetry (the axis along the length of the wire) and therefore the excitations are characterized by a 1D wave vector. The straightforward modification of Bloch's theorem in this case yields

$$\psi(x, y, z) = \exp\left(\mathrm{i}q_z z\right) U_{q_z}(x, y, z), \tag{1.29}$$

where it is assumed here that the z-axis is along the translational symmetry axis.

Finally, we may have structures that are finite in all three dimensions, such as a small cuboid or a sphere. These have no translational symmetry (so Bloch's theorem does not apply) and they may be labelled as being 0D, such as the 'quantum dots' that have been of particular interest for semiconductors or flat 'platelets' or 'disks' for magnetic materials (see, e.g., [18, 19]). The low-dimensional structures mentioned here are illustrated schematically using examples in figure 1.4(a).

1.2.2 Multilayers and superlattices

If more than one material is utilized, then more elaborate cases of nanostructures can arise than those in the previous subsection. One simple possibility is to build up multilayers with alternating thin films of two materials, denoted as A and B, to form an $ABABAB\cdots$ pattern of growth on a substrate material. Such an example is provided in figure 1.4(b) for the materials shown in different colours. The simplest case would be a bilayer AB, but multilayers with a large number of layers (e.g., hundreds or more) can be fabricated. In all cases these systems would have the property of translational symmetry for lattice directions parallel to the planar surfaces and interfaces. Thus the 2D Bloch's theorem in equation (1.28) still applies, with the only essential difference being that the term $U_{\mathbf{q}_\parallel}(\mathbf{r}_\parallel, z)$ may have a more complicated dependence on z. There may, for example, be excitations that are localized only near the interfaces between A and B layers.

Another aspect of multilayers that makes them of special interest occurs when all the A layers have identical properties (composition, thickness, etc) to one another and likewise for all the B layers. The structure then consists of repeats of the same basic AB building block. If there is a large number of these repeats, then a new symmetry operation emerges corresponding to translations in the z-direction through a periodicity length $D = d_A + d_B$, where d_A and d_B denote the thicknesses of the individual A and B layers. We then have an example of a *periodic superlattice*, for which the inbuilt artificial periodicity in the z-direction may be associated with a new 1D Brillouin zone that extends in reciprocal space from $-\pi/D$ to π/D. Since D is typically much larger than the lattice parameter a of either constituent material, this new Brillouin zone is smaller than the crystal Brillouin zone. This can have striking consequences for the excitations that propagate as waves in the perpendicular (z-)direction of the superlattice. A smaller Brillouin zone can sometimes be advantageous as regards the experimental techniques for studying the excitations and it also leads to a 'folding' of the dispersion curves, as we will discuss through examples in section 1.5 and later chapters.

The concept of a superlattice was originally introduced by Esaki and Tsu [20] for ultrathin semiconductor multilayers where the layer thicknesses were less than the electron mean free path, but currently the term is applied more generally for multilayers that are either periodic or are generated according to certain mathematical rules. In the former category we may also have periodic arrangements with three (or more) components, $ABCABCABC\cdots$ for example, as well as the two-component superlattice described above. In the latter category we may include *quasi-periodic superlattices* (see, e.g., [21], where the sequencing of layers along the growth direction is quasi-periodic in

the sense that it involves two different fundamental periods whose ratio is an irrational number. One way to achieve this is through the Fibonacci sequence of numbers, $\{F_n\}$ with integer $n = 0, 1, 2, \ldots$, that is defined by the recursion relation

$$F_{n+2} = F_{n+1} + F_n, \tag{1.30}$$

with the initial conditions $F_1 = F_0 = 1$. It is straightforward to prove that as n becomes very large ($n \to \infty$) the ratio F_{n+1}/F_n tends to the value $(1 + \sqrt{5})/2 \simeq 1.618$ which is known as the golden mean. For the application to Fibonacci superlattices some fundamental property of the layered growth is developed by analogy with equation (1.30), as explained later. The excitations in quasi-periodic superlattices have novel properties (e.g., regarding their localization, multifractal behaviour, etc) that make them of special interest [22].

1.2.3 Laterally patterned structures

By contrast with the previous subsection we will now discuss some artificial nanostructures produced by a lateral arrangement (usually periodic) of elements such as that represented in figure 1.4(c). This shows an alternating sequence of stripes of two different materials deposited side-by-side on a planar surface, rather than stacked vertically. Interest in such structures was given impetus in 1987 through seminal work by Yablonovitch [23] and John [24], who studied artificial electromagnetic materials, typically in low dimensions, that have periodic modulation of the refractive index. This was originally undertaken with a view to control the propagation, localization and scattering of light, and led to periodic structures known as either *photonic crystals* or alternatively *photonic band-gap materials* for applications in optoelectronics. Some consequences for the photonic band structure in periodic cases are developed in section 1.5.

More recently, aided by advances in materials growth and fabrication on the submicron scale, other types of laterally patterned materials have been utilized to study phonons (hence *phononic crystals*), SWs or magnons (*magnonic crystals*; MCs) and plasmons (*plasmonic crystals*), among others. One of the characteristic features of these materials is the tailoring of the band structure of the excitations and the forbidden-frequency gaps (or band gaps) in the spectrum. We shall discuss these cases in more detail in later chapters. Just as with the superlattices in the previous subsection, effects will arise due to a modified Bloch's theorem and mini-Brillouin zones due to the artificial periodicity. The example depicted in figure 1.4(c) with a striped array is a 1D crystal in the lateral plane, but 2D patterning (as with a chess or checker board array) provides another case of interest.

1.3 Experimental techniques for dynamic properties

Although a wide range of different physical phenomena will contribute to the dynamic properties of materials, many of the same experimental techniques will be applicable. This will also be the case as regards the theoretical tools needed to study the excitations and so it is useful to give a broad introduction in this chapter and to

provide some general references. The experimental aspects are covered first in this section and the theoretical topics will be described in section 1.4.

We will emphasize here the techniques that are most useful as regards the dynamical properties and characterization of the excitations. These include inelastic light scattering, inelastic particle scattering, electromagnetic techniques and magnetic (or spin) resonance methods, etc. A fuller account can be found in [4]. We do not describe here the sample growth and preparation techniques, or the analytical tools for surface and interface structural properties, since these are not the focus of this book and they have been extensively covered elsewhere (see, e.g., [19, 25, 26]).

Both Raman and Brillouin scattering of light by dense media involve an inelastic process whereby the incident light of angular frequency ω_{I} (or a photon of energy $\hbar\omega_{\mathrm{I}}$) and wave vector k_{I} interact with the medium by creating or absorbing an excitation and producing a scattered light beam. Although these effects were discovered in the early part of the 20th century, it was not until much later with the advent of the laser and other technical developments that they were widely used for studying bulk and surface excitations. The essential difference between the two techniques lies in the method used to analyse the frequency of the scattered light; this involves a grating spectrometer for Raman scattering (RS) (where the wavenumber shifts of the light are typically in the range 5–4000 cm^{-1}) and a Fabry–Pérot interferometer for Brillouin scattering (where the wavenumber shifts are below about 5 cm^{-1}). Note that a wavenumber shift of 1 cm^{-1} corresponds to a 29.98 GHz frequency shift. We label the excitation by ω and $\mathbf{q}$ and the scattered light by ω_{S} and $\mathbf{k}_{\mathrm{S}}$, and the two possible processes (known as Stokes and anti-Stokes scattering) are represented schematically in figure 1.5. When the light scattering takes place in a bulk (effectively infinite) 3D transparent material the energy and momentum are conserved and so

$$\hbar\omega_{\mathrm{I}} = \hbar\omega_{\mathrm{S}} \pm \hbar\omega, \qquad \hbar\mathbf{k}_{\mathrm{I}} = \hbar\mathbf{k}_{\mathrm{S}} \pm \hbar\mathbf{q}, \tag{1.31}$$

where the upper (lower) signs correspond to the Stokes (anti-Stokes) case. The dispersion relations for the incident and scattered light yield $|k_{\mathrm{I}}| = \eta_{\mathrm{I}}\omega_{\mathrm{I}}/c$ and $|\mathbf{k}_{\mathrm{S}}| = \eta_{\mathrm{I}}\omega_{\mathrm{S}}/c$, where η_{I} and η_{S} denote the corresponding values of the refractive index. The above relations, together with the conservation properties in equation (1.31), imply that only excitations with wave vectors near the centre of the Brillouin zone in a bulk material are excited.

There are several modifications for the application of light scattering in low-dimensional and/or optically absorptive materials. First, with thin films and

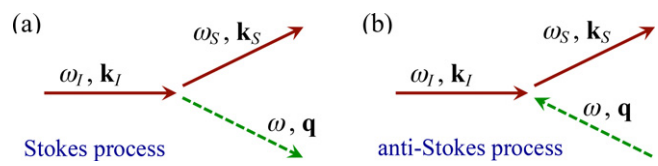

Figure 1.5. Representation of the (a) Stokes and (b) anti-Stokes processes of inelastic light scattering. The incident and scattered photons are depicted by solid lines and the created or absorbed excitation by a dashed line.

multilayers on the one hand, or nanowires and nanowire arrays on the other, the conservation of momentum will apply only in the 2D or 1D direction(s) where the system has translational symmetry. In the other dimension(s) there will be a spread of wave-vector components for the excitation, implying a spread of frequencies in the measured spectrum. The extent to which this occurs depends on the optical absorption (or imaginary part of the refractive index) in the material. If the absorption is large, which is typical for metals and some semiconductors, the light will penetrate only close to the surface of the material, so light scattering can be sensitive to surface properties and to the excitations localized there. In the case of 0D materials (or dots) none of the wave-vector components will be conserved. As well as providing information about the frequencies, light scattering also probes the intensities of the excitations. The scattering cross section is, in fact, related to the correlations between components of the electric field for the scattered light and this provides a connection between theory and experiment, as we describe later. Some general references for inelastic light scattering are [27] (mainly in bulk materials), [28, 29] (mainly in thin films and multilayers) and [30] (mainly in other low-dimensional materials).

Next we turn to the inelastic scattering of particles by the crystal excitations. In principle this process may involve larger momentum changes than encountered with light, so by contrast particle scattering may be useful for probing excitations throughout the entire Brillouin zone, depending on the type of particle involved. In electron energy loss spectroscopy (EELS), and in its high-resolution variant (HREELS), a beam of electrons is scattered from the surface of a material, as reviewed in [31, 32]. A typical geometry for the scattering of particles from a planar surface is shown in figure 1.6, where a surface excitation such as a phonon is emitted or absorbed in the process. The condition for conservation of energy yields

$$E_{\mathrm{I}} = E_{\mathrm{S}} \pm \hbar\omega, \tag{1.32}$$

where we follow the notation in figure 1.6 and the upper (lower) sign refers to the creation (annihilation) case for the excitation. The other scattering condition corresponds to the conservation of the momentum component in the direction parallel to the surface plane, giving

$$|\hbar k_{\mathrm{I}} \sin\theta_{\mathrm{I}} - \hbar k_{\mathrm{S}} \sin\theta_{\mathrm{S}}| = \hbar q_{\parallel}. \tag{1.33}$$

Also, we have the classical energy–momentum relations $E_{\mathrm{I}} = (\hbar k_{\mathrm{I}})^2/2M$ and $E_{\mathrm{S}} = (\hbar k_{\mathrm{S}})^2/2M$ with M denoting the particle mass. Generally for EELS or

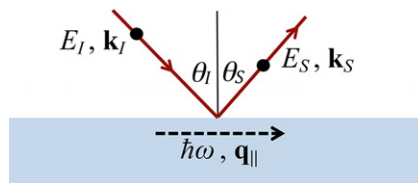

Figure 1.6. Geometry for inelastic particle scattering from a planar surface of a material, where the incident and scattered beam are in the same vertical plane.

HREELS we can approximate by assuming $E_I \gg \hbar\omega$, which is usually well satisfied (e.g., if $E_I \sim 100$ eV and $\hbar\omega \sim 100$ meV), implying $|\mathbf{k}_S| \simeq |\mathbf{k}_I| \equiv k_I$. For the same reason we can also ignore Umklapp processes in equation (1.33). It follows that, by varying the angles θ_I and θ_S, the in-plane wave vector can be varied across its 2D Brillouin zone and the ω-versus-$\mathbf{q}_{\|}$ dispersion relation for the surface excitation can be investigated. An example of this type of analysis is provided by the work of Lehwald *et al* [33] for phonons localized at a Ni surface. Spin-polarized EELS has been used for magnetic excitations at surfaces [34]. It involves employing a spin-polarized incident electron beam together with a polarization analyser in the scattered beam.

The inelastic scattering of particles that are much heavier than electrons allows for larger momentum changes and hence offers the prospect of making it easier (in principle) to study excitations with large wave vectors. Inelastic neutron scattering is well established for studying bulk excitations. However, neutrons interact only very weakly with materials and have macroscopically large penetration depths, so this method is relatively insensitive to surface effects. This drawback may be mitigated if the surface or interface area is effectively increased (e.g., by using a short-period superlattice) or if a neutron beam is used at grazing incidence to a surface (see, e.g., [35]). However, in the context of *surface* excitations, the inelastic scattering of small neutral atoms, such as He atoms, has proved to be more useful. The He atoms at suitable incident energies (e.g., of order 20 meV) will be scattered back from a surface by essentially just the first monolayer (ML) of the material. Also the atoms in the incident beam will have a de Broglie wavelength ($=h/\sqrt{2ME_I}$) that is typically comparable with the lattice constant, so the entire 2D Brillouin zone can be studied. The technique was pioneered by Brusdeylins *et al* [36] using time-of-flight spectroscopy to study surface phonons. The basic equations for the scattering are essentially the same as for EELS, equations (1.32) and (1.33), except that it is no longer true that $k_I \simeq k_S$ because of the larger particle mass here. In the case of a 90° scattering geometry (when $\theta_I + \theta_S = \pi/2$ in figure 1.6) it is straightforward to show that ω and $q_{\|}$ are related by

$$\omega = \frac{\hbar^2 k_I^2}{2M}\left[\left(\frac{q_{\|} + k_I \sin\theta_I}{k_I \cos\theta_I}\right)^2 - 1\right]. \tag{1.34}$$

This allows the dispersion relation of a surface excitation to be deduced.

To conclude this section we briefly mention some experimental techniques that are specific to certain types of excitations. Others will be mentioned in later chapters. Magnetic resonance techniques are widely used for excitations in magnetic materials, both in the bulk and in low-dimensional geometries (see [29] for a review). At low power levels a microwave magnetic field (in a direction transverse to the magnetization) will couple linearly to the zero wave-vector SWs (magnons) in a ferromagnet, leading to the ferromagnetic resonance (FMR) condition when the frequencies of the field and excitation match. The analogous effect in antiferromagnets is called antiferromagnetic resonance (AFMR) and typically occurs at higher frequencies. In SW resonance (SWR) in ferromagnetic thin films the technique is used to excite selectively the standing SWs across the film thickness

that have small but nonzero wave vectors. At higher power levels the oscillating (or 'pumping') magnetic field can be used to promote various NL SW processes in ferromagnets, as we will discuss in chapter 7.

Another area involving specialized techniques occurs with excitations that generate electromagnetic waves. These can be studied using optical methods that employ, for example, evanescent wave coupling in the region near closely positioned interfaces between media of different refractive index. This is the basis of the method of attenuated total reflection (ATR), which has been successfully applied to plasmons and polaritons (see chapters 4 and 5). Evanescent wave properties are also exploited in scanning near-field optical microscopy, which is a form of scanning probe microscopy.

1.4 Theoretical methods for dynamic properties

1.4.1 Equations of motion for excitations

Some of the theoretical considerations have already been mentioned in earlier parts of this chapter, particularly in subsection 1.1.2, where we presented some simple examples of linear and NL excitations. There we emphasized the role of an equation of motion for the excitation amplitude, e.g., Maxwell's wave equation for the electric field as in equation (1.19), along with boundary conditions and/or the use of Bloch's theorem to deal with spatial periodicity where needed.

From such an approach one would normally be able to deduce the excitation frequency and hence a dispersion relation, as well as information about the spatial variation in the case of a localized excitation. As discussed earlier in section 1.2, a bulk excitation will depend on a 3D wave vector $\mathbf{q}$, whereas a surface or interface excitation at a planar interface will be characterized by a 2D wave vector $\mathbf{q}_{||}$ and one or more attenuation factors (or decay lengths). Other considerations apply in 1D and 0D systems, as mentioned before. Calculating the excitation frequencies in a low-dimensional system normally involves having a set of *homogeneous* equations of motion satisfied by the amplitude variable(s) in the different parts of the system. These equations may either be differential equations if a macroscopic (or continuum) approach is being followed, as in the previous examples given for electromagnetic excitations, or finite-difference equations if a microscopic approach is used, as in a discrete-lattice model. Both approaches will be used throughout the following chapters. Also, in some cases, numerical simulation packages have been developed to carry out these calculations. An example is the Object Oriented MicroMagnetic Framework (OOMMF) project at the US National Institute of Standards and Technology, which is applicable to studying a range of properties of micromagnetic low-dimensional systems [37].

It is useful to briefly consider some other examples that involve a homogeneous equation of motion, apart from the electromagnetic one given previously. First we take the case of an infinite, isotropic elastic medium with a longitudinal vibrational wave (an acoustic phonon) propagating in one direction, which we label as the z-direction. If we denote $u(z, t)$ as the local displacement in the z-direction of the medium, ρ as the uniform density of the medium and v_L as the longitudinal sound

wave velocity, the usual linear wave equation with weak damping (constant $\gamma > 0$) included is (see, e.g., [1, 3])

$$\rho\frac{\partial^2 u}{\partial t^2} + \rho\gamma\frac{\partial u}{\partial t} - \rho {v_{\mathrm{L}}}^2\frac{\partial^2 u}{\partial z^2} = 0. \tag{1.35}$$

A solution is easily found by taking $u(z, t) \propto \exp[\mathrm{i}(qz - \omega t)]$ which yields the condition $\omega^2 + \mathrm{i}\omega\gamma = {v_{\mathrm{L}}}^2 q^2$. In the limit of zero damping ($\gamma \to 0$) this gives the usual acoustic-phonon dispersion relation $\omega = v_{\mathrm{L}} q$, as expected.

When a discrete-lattice approach is followed, leading to finite-difference equations for the spatial variables instead of differential equations, some special techniques are useful. One of these is the *tridiagonal matrix* (TDM) method, which is useful for surface and interface problems when the interactions are short range, often just between nearest neighbours. A general outline of the method is given in the appendix and some applications are discussed later, e.g., for the lattice dynamics of phonons in chapter 2 and for exchange-dominated SWs in ferromagnets in chapter 3.

A somewhat different situation will occur if the excitation is described in terms of a quantum-mechanical operator, rather than a classical amplitude as above. This will be so, for example, in the case of a magnetic system consisting of a lattice of atoms where each atom is associated with a spin angular-momentum operator (see chapter 3). If the quantum-mechanical system is represented by a Hamiltonian H, then the equation of motion for any operator A of the system is obtained from [38]

$$i\hbar\frac{\mathrm{d}A}{\mathrm{d}t} = [A, H], \tag{1.36}$$

where $[A, H] \equiv (AH - HA)$ denotes the commutator between the two operators. For simplicity we shall henceforth usually take units such that $\hbar = 1$. Equation (1.36) may be either a linear or NL equation in A, depending on whether the outcome of evaluating the commutator of the operator A (for the excitation) with the Hamiltonian gives an expression that is linear in A or has some other more complicated dependence. Examples of both cases will arise later in this book, but it is probably most clearly illustrated for magnons in ferromagnets (see chapters 3 and 7).

1.4.2 Linear-response theory for excitations

In many cases we are interested in other properties of the excitations apart from their dispersion relations. For example, we may need to know the relative statistical weighting (or spectral intensity) of the excitations or to find a scattering cross section to compare with experiment. This information can be provided by linear-response theory and we will now outline this method and then illustrate it with an example. The basis of the method is to calculate the response of the system to a small applied stimulus, taking care to choose the appropriate classical or quantum variables (relating to the excitation being studied). The *response functions* provide not only the dispersion relations for the relations but also the intensity-related information mentioned above. General accounts of linear-response theory are to be found, for example, in [4, 39] where the connection to Green functions is also explained.

A comprehensive treatment in the context of low-dimensional systems can be found in [40]. Here (and also in the appendix) we will present, for later reference, only the important results.

We suppose that a time-dependent perturbation described by Hamiltonian $H_{\mathrm{I}}(t) = -Bf(t)$ is applied to the system, where $f(t)$ is a scalar external field that couples linearly to a system variable denoted by the operator B. An example is when B is a displacement from equilibrium in an elastic medium and $f(t)$ is a mechanical force. The total Hamiltonian can be written as

$$H = H_0 - Bf(t), \tag{1.37}$$

where H_0 denotes the Hamiltonian for the unperturbed system, taken to be in thermal equilibrium at time $t = -\infty$. At any later time the response of the system can be expressed in terms of the change $\bar{A}(t)$ produced in any other system variable corresponding to an operator denoted as A. The procedure for doing this is outlined in the appendix and the main conclusion is that

$$\bar{A}_\omega = \langle\langle A; B\rangle\rangle_\omega \, F(\omega), \tag{1.38}$$

where $\bar{A}_\omega$ and $F(\omega)$ are defined to be the frequency Fourier components of $\bar{A}(t)$ and $f(t')$, respectively. This result holds within a linear approximation in terms of the perturbation term and the proportionality factor written as $\langle\langle A; B\rangle\rangle_\omega$ in equation (1.38) is identified as the Fourier component of the Green function that describes correlations between the operators A and B. The above result establishes the role of Green functions as linear-response functions, in the sense that they are just the same as the proportionality factor between an applied stimulus to the system, represented by $F(\omega)$, and the response that it produces, represented by $\bar{A}_\omega$. The formal definitions and some basic properties of Green functions are given in the appendix.

In order to illustrate the formalism for response functions and Green functions, we return to the physical example of excitations in an infinite elastic medium considered earlier in this section. The homogeneous equation of motion for the displacement $u(z)$ for a longitudinal acoustic (LA) wave in the z-direction was given by equation (1.35), to which we now add a driving term (a perturbation) which is chosen to represent a harmonic point force at position z' in the system, i.e., we take

$$f(z, t) = \left(f_0/A_0\right)\exp(-\mathrm{i}\omega t)\delta(z - z'), \tag{1.39}$$

where f_0 is an amplitude and A_0 is the area presented by the system in the xy-plane. The total interaction energy with the system is

$$\begin{aligned} H_{\mathrm{I}}(t) = -\int\int\int u(z)f(z, t)\mathrm{d}x\ \mathrm{d}y\ \mathrm{d}z &= -f_0\exp(-\mathrm{i}\omega t)\int u(z)\delta(z - z')\mathrm{d}z \\ &= -f_0\exp(-\mathrm{i}\omega t)u(z'), \end{aligned} \tag{1.40}$$

so it takes the general form assumed earlier. The equation of motion on generalizing (1.35) becomes

$$\rho\frac{\partial^2 u}{\partial t^2} + \rho\gamma\frac{\partial u}{\partial t} - \rho{v_{\mathrm{L}}}^2\frac{\partial^2 u}{\partial z^2} = \frac{f_0}{A_0}\exp(-\mathrm{i}\omega t)\delta(z - z'). \tag{1.41}$$

As anticipated, the outcome is that we now have an *inhomogeneous* differential equation. We may first take a common time dependence such as $\exp(-\mathrm{i}\omega t)$, leaving as the equation for the spatial dependence

$$\frac{\mathrm{d}^2u}{\mathrm{d}z^2} + q^2u = -\frac{f_0}{\rho v_\mathrm{L}^2 A_0}\delta(z - z'), \tag{1.42}$$

where the complex q^2 is defined in the same way as following equation (1.35). We seek the solution that is bounded as $z - z' \to \pm\infty$ and has the correct behaviour as $z - z' \to 0$. It may easily be verified that the result is

$$u(z) = \frac{\mathrm{i}f_0}{2\pi\rho v_\mathrm{L}^2 A_0}\exp(\mathrm{i}q|z - z'|). \tag{1.43}$$

In the spirit of linear-response theory this is the driven equation for $u(z)$ due to a harmonic force applied at point $z = z'$. From equation (1.38) we obtain the Green function as

$$\langle\langle u(z);\, u(z')\rangle\rangle_\omega = \frac{\mathrm{i}}{2\pi\rho v_\mathrm{L}^2 A_0}\exp(\mathrm{i}q|z - z'|). \tag{1.44}$$

Since the above result is a function of $z - z'$, as expected for a system with translational symmetry, we can re-express it by making a Fourier transform from the spatial variables to a wave-vector component k in the z-direction:

$$\langle\langle u;\, u)\rangle\rangle_{k,\omega} \equiv \int_{-\infty}^{\infty}\langle\langle u(z);\, u(z')\rangle\rangle_\omega \mathrm{e}^{-\mathrm{i}k(z-z')}\mathrm{d}(z - z') = \frac{1}{2\pi A_0\left(v_\mathrm{L}^2k^2 - \omega^2 - \mathrm{i}\omega\gamma\right)}. \tag{1.45}$$

The last step for this result is accomplished by splitting the range of integration into two parts with $z < z'$ and $z > z'$. We note that the condition for the energy denominator to be zero yields the dispersion relation $\omega_k = v_\mathrm{L}k$ for the excitation (an acoustic phonon) if the damping is ignored. This illustrates a general property for the denominator of Green functions. Finally we may use equation (1.45) together with the fluctuation-dissipation theorem in the appendix to obtain $\langle|u|^2\rangle_{k,\omega}$ which is a measure of the spectral intensity (or mean-square amplitude) of the excitation as a function of k and ω. A numerical example of the result appears in figure 1.7, where the peaks occur for ω close to $\pm\omega_k$ provided the damping is relatively small ($\gamma \ll \omega_k$). The peaks are unequal in height due to the statistical-mechanical weighting, which depends on the temperature T. This has consequences, for example, regarding the difference in intensities observed between Stokes and anti-Stokes peaks in inelastic light scattering, as we will discuss in chapters 2 and 3.

1.5 Photonic band gaps in periodic structures

We have already briefly mentioned periodic structures in subsections 1.2.2 and 1.2.3, which are typically formed from two or more materials, either as superlattices or as lateral arrays. The bands of excitations in such structures (i.e., their frequency versus wave-vector relationships) can be very complicated in general and particular

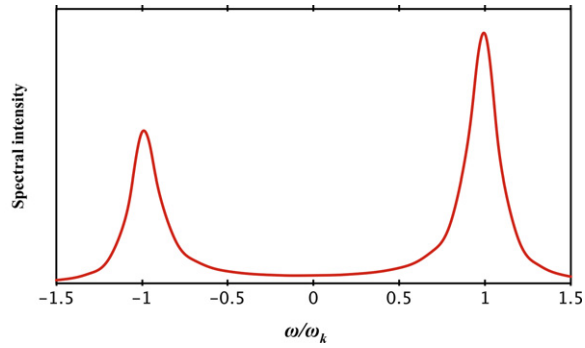

Figure 1.7. The spectral intensity $\langle |u|^2 \rangle_{k,\omega}$ versus reduced frequency ω/ω_k for the acoustic phonons in an infinite elastic medium (see the text). We denote $\omega_k \equiv v_L k$ for a fixed value of wave-vector component k. The assumed numerical values of the parameters correspond to dimensionless $k_B T/\hbar\omega_k = 2$ and $\gamma/\omega_k = 0.2$.

features may sometimes arise, such as the appearance of band gaps at the mini-Brillouin-zone boundaries mentioned earlier. The properties for the occurrence and manipulation of such bands have led to the tremendous interest in *band-gap materials*, initially in the photonics case in optics (see [41] for a thorough review) but subsequently for other excitations as well. In this introductory chapter we present a simple formulation for a 1D photonic band-gap material (a photonic crystal) and discuss some extensions to 2D or 3D. This treatment will serve as a template for carrying out other calculations for periodic (and quasi-periodic) structures in the later chapters.

1.5.1 Bulk-slab model

Here we consider alternating layers of medium A and medium B to form the superlattice structure depicted in figure 1.8. The layer thicknesses are d_A and d_B, both assumed to be large compared with the atomic lattice parameters of the materials. The length associated with the artificial periodicity is $D = d_A + d_B$ and so the 1D wave vector Q (the so-called Bloch wave vector) in the z-direction associated with this translational symmetry has a first Brillouin zone corresponding to $-\pi/D < Q \leqslant \pi/D$. Further it will be assumed that the dielectric functions are ε_A and ε_B, taken for simplicity to be the bulk dielectric constants (independent of the excitation angular frequency ω). This is sometimes referred to as the *bulk-slab model* of a superlattice.

We now employ standard results from electromagnetism for the optical wave propagation in the layers, taken to be in the xz plane. There are basically two cases, depending on whether the waves have s-polarization (with electric-field vector $\mathbf{E}$ in the y-direction) or p-polarization (with $\mathbf{E}$ in the xz-plane). The wave-vector component Q enters into the calculations through Bloch's theorem in the form

$$\mathbf{E}(z + D) = \exp(\mathrm{i}QD)\mathbf{E}(z). \tag{1.46}$$

Also all field components will be taken to have dependences on x and t as $\exp(\mathrm{i}q_x x - \mathrm{i}\omega t)$, where for completeness we have included a wave vector q_x in the x-direction to allow for oblique incidence of the optical waves at each interface.

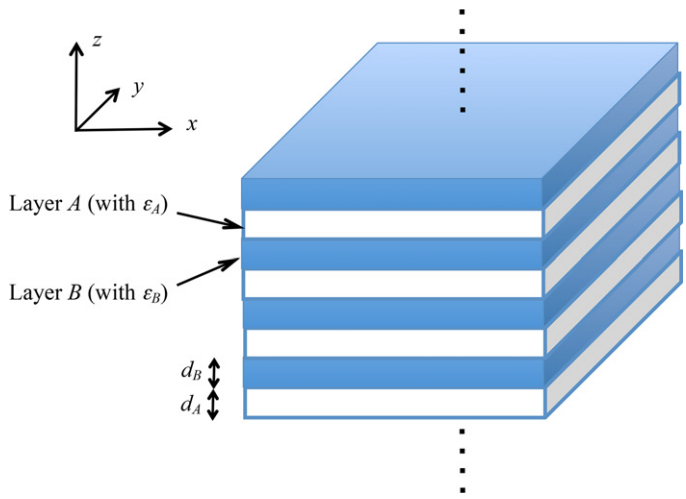

Figure 1.8. Geometry and notation for the calculation of the photonic (optical) band structure of a two-component alternating periodic superlattice. The wave propagation directions are taken to be in the xz plane.

The calculation for s-polarization will be shown first. The solution of the wave equation (1.19) for E_y in any layer will be a superposition of a forward- and a backward-travelling wave in the z-direction. Alternative forms can be written down, depending on whether the phases are taken relative to the lower (L) or upper (U) interface of each layer, giving

$$\begin{aligned} E_y &= a_l^{\mathrm{L}} \exp\left[\mathrm{i}q_{Az}(z - lD)\right] + b_l^{\mathrm{L}} \exp\left[-\mathrm{i}q_{Az}(z - lD)\right] \\ &= a_l^{\mathrm{U}} \exp\left[\mathrm{i}q_{Az}(z - lD - d_A)\right] + b_l^{\mathrm{U}} \exp\left[-\mathrm{i}q_{Az}(z - lD - d_A)\right] \end{aligned} \tag{1.47}$$

in an A layer (with $lD \leqslant z \leqslant lD + d_A$) where q_{Az} must satisfy

$$q_{Az}^2 + q_x^2 = \varepsilon_A \omega^2 / c^2. \tag{1.48}$$

For the field in the adjacent layer B in the same cell l (with $lD + d_A \leqslant z \leqslant (l+1)D$) and with q_{Bz} defined similarly to equation (1.48), we have

$$\begin{aligned} E_y &= d_l^{\mathrm{L}} \exp\left[\mathrm{i}q_{Bz}(z - lD - d_A)\right] + e_l^{\mathrm{L}} \exp\left[-\mathrm{i}q_{Bz}(z - lD - d_A)\right] \\ &= d_l^{\mathrm{U}} \exp\left[\mathrm{i}q_{Bz}(z - (l+1)D)\right] + e_l^{U} \exp\left[-\mathrm{i}q_{Bz}(z - (l+1)D\right]. \end{aligned} \tag{1.49}$$

Using a matrix notation the amplitudes in equation (1.47) are related by

$$\left|u_l^{\mathrm{U}}\right\rangle = F_A \left|u_l^{\mathrm{L}}\right\rangle, \tag{1.50}$$

where we denote

$$\left|u_l^{\mathrm{L,U}}\right\rangle = \begin{pmatrix} a_l^{\mathrm{L,U}} \\ b_l^{\mathrm{L,U}} \end{pmatrix} \tag{1.51}$$

and F_A is a 2×2 matrix given by

$$F_A = \begin{pmatrix} f_A & 0 \\ -0 & f_A^{-1} \end{pmatrix} \tag{1.52}$$

with phase term $f_A = \exp(\mathrm{i}q_{Az}d_A)$. Likewise for the other layer we write

$$\left|w_l^{\mathrm{U}}\right\rangle = F_B\left|w_l^{\mathrm{L}}\right\rangle \tag{1.53}$$

with analogous notations and definitions.

The electromagnetic boundary conditions at the $z = lD + d_A$ and $z = (l + 1)D$ interfaces require that E_y and H_x are continuous (implying that E_y and $\partial E_y/\partial z$ are continuous). These can be used to give additional relationships between the column matrices of coefficients. The results can eventually be expressed in matrix form as

$$X_A\left|u_l^{\mathrm{U}}\right\rangle = X_B\left|w_l^{\mathrm{L}}\right\rangle \qquad \text{and} \qquad X_B\left|w_l^{\mathrm{U}}\right\rangle = X_A\left|u_{l+1}^{\mathrm{L}}\right\rangle, \tag{1.54}$$

where

$$X_i = \begin{pmatrix} 1 & 1 \\ q_{iz} & -q_{iz} \end{pmatrix}, \quad i = A, B. \tag{1.55}$$

The equations (1.50), (1.53) and (1.54) may now be combined to give

$$\left|u_{l+1}^{\mathrm{L}}\right\rangle = T\left|u_l^{\mathrm{L}}\right\rangle, \tag{1.56}$$

which relates amplitudes in cell l to the equivalent part in cell $l + 1$ and introduces the *transfer matrix* T given by

$$T = X_A^{-1}X_BF_BX_B^{-1}X_AF_A. \tag{1.57}$$

The transfer matrix has some useful properties, as we now explain. First, it is unimodular in the sense that $\det T = 1$, which can be proved from the form of matrix products in equation (1.57). Second, the statement of Bloch's theorem in equation (1.46) is equivalent to

$$\left|u_{l+1}^{\mathrm{L}}\right\rangle = \exp(\mathrm{i}QD)\left|u_l^{\mathrm{L}}\right\rangle \tag{1.58}$$

and therefore we have the property that

$$\left[T - \exp(\mathrm{i}QD)I\right]\left|u_l^{\mathrm{L}}\right\rangle = 0, \tag{1.59}$$

where I is the unit 2×2 matrix. There is a similar equation obtained by relating $|u_{l-1}^{\mathrm{L}}\rangle$ to $|u_l^{\mathrm{L}}\rangle$, yielding

$$\left[T^{-1} - \exp(-\mathrm{i}QD)I\right]\left|u_l^{\mathrm{L}}\right\rangle = 0. \tag{1.60}$$

By adding equations (1.59) and (1.61) we find

$$\left[T + T^{-1} - 2\cos(QD)I\right]\left|u_l^{\mathrm{L}}\right\rangle = 0, \tag{1.61}$$

which holds for any cell l. Therefore, from the property that $(T + T^{-1}) = (\mathrm{tr}T)I$, where 'tr' denotes the trace, we must have

$$\cos(QD) = \frac{1}{2}\,\mathrm{tr}\;T. \tag{1.62}$$

This is a general result, providing an implicit dispersion relation for the excitation frequencies in terms of the Bloch wave vector Q and the transfer matrix T.

Explicit evaluation shows that the diagonal elements of T in the present example are

$$\begin{aligned} T_{11} &= f_A\left[f_B\left(q_{Az} + q_{Bz}\right)^2 - f_B^{-1}\left(q_{Az} - q_{Bz}\right)^2\right]\Big/ 4q_{Az}q_{Bz}, \\ T_{22} &= f_A^{-1}\left[f_B^{-1}\left(q_{Az} + q_{Bz}\right)^2 - f_B\left(q_{Az} - q_{Bz}\right)^2\right]\Big/ 4q_{Az}q_{Bz}. \end{aligned} \tag{1.63}$$

When these results are substituted into equation (1.62) we find after some algebraic manipulation that the dispersion relation in this case of s-polarization is

$$\cos(QD) = \cos\left(q_{Az}d_A\right)\cos\left(q_{Bz}d_B\right) - g_{\mathrm{s}}\sin\left(q_{Az}d_A\right)\sin\left(q_{Bz}d_B\right) \tag{1.64}$$

where

$$g_{\mathrm{s}} = \frac{1}{2}\left(\frac{q_{Bz}}{q_{Az}} + \frac{q_{Az}}{q_{Bz}}\right). \tag{1.65}$$

The calculation for the case of p-polarization is very similar and it is found that equation (1.64) is still applicable provided g_{s} is replaced by g_{p} where

$$g_{\mathrm{p}} = \frac{1}{2}\left(\frac{\varepsilon_B q_{Az}}{\varepsilon_A q_{Bz}} + \frac{\varepsilon_A q_{Bz}}{\varepsilon_B q_{Az}}\right). \tag{1.66}$$

The dispersion equation in the general form represented by (1.64) occurs commonly for excitations in periodic structures, as we will see in later chapters. It is sometimes called the *Rytov equation*, since its first derivation is attributed to Rytov in the context of acoustic waves [42]. Full discussion of the results for the above optical superlattice, or photonic crystal, can be found in [41, 43]. We present a numerical example of a dispersion relation in figure 1.9 in the special case of normal incidence where $q_x = 0$ and the distinction between s- and p-polarization vanishes. The plot is in dimensionless units for frequency ω versus Q. In the reduced-zone scheme used here the dispersion curves are 'folded back' and gaps open up at $QD = 0$ and π. In this example the band gaps (or stop bands) are relatively large because we have assumed a significant difference, or mismatch, between the dielectric constants

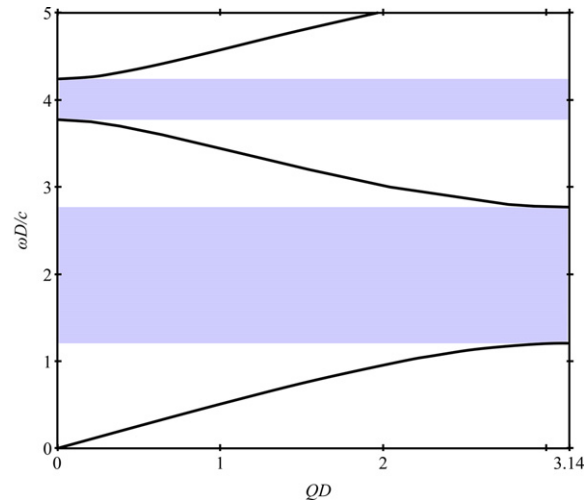

Figure 1.9. Dispersion curves of frequency (in terms of $\omega D/c$) versus Bloch wave vector (in terms of QD) for normal-incidence optical waves in a 1D photonic crystal consisting of a two-component alternating periodic superlattice. The assumed parameters are $d_A = d_B = 0.5D$, $\varepsilon_A = 3$ and $\varepsilon_B = 2$. The PBGs are shown as the shaded areas.

of adjacent layers. If the dielectric constants are taken to be close in value, the gaps shrink to a small value.

Finally we remark that the transfer-matrix method can straightforwardly be modified to apply other types of excitations, as well as to study the localized surface and/or interface modes (when they exist) in periodic and quasi-periodic structures that are either semi-infinite or finite in extent (in the z-direction). Results to illustrate this will be covered in some of the later chapters.

1.5.2 Photonic crystals in 2D and 3D

In the previous subsection it was demonstrated that stop bands would arise as a result of 1D periodicity in a superlattice. The interesting question arises as to whether it is possible to achieve 2D, or even 3D, arrays that would have stop bands or band gaps for optical signals at some frequencies and for both polarizations. The first investigations relating to this were made by Yablonovitch [23] in 1987, while related light localization studies were carried out around the same time by John [24]. A motivation for these early studies was the realization that a stop band with the properties mentioned would prohibit spontaneous emission of radiation in optical transitions and this could be utilized for semiconductor lasers and devices. However, subsequently a wide range of other quantum-optical device applications has emerged and an excellent reference is the book by Joannopoulos *et al* [41], which also covers the modelling techniques used to calculate the stop bands and the transmission characteristics.

The first realization of a full photonic band gap (PBG) material was due to Yablonovitch *et al* [44] who formed a structure that absorbed 15 GHz radiation for all spatial directions and polarizations. It was made by drilling air holes at various

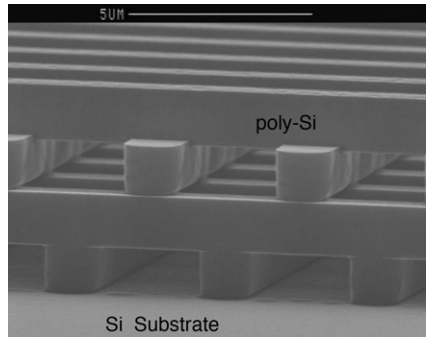

Figure 1.10. SEM of a 3D photonic crystal with a 'woodpile' structure. The rods are made of polycrystalline Si with widths 1.2 μm. The stacking sequence shown here repeats itself every four layers. Scale bar, 5 μm. After Lin *et al* [45].

angles into a dielectric block. Such an arrangement, whilst effective, would be impractical for scaling to the higher frequencies (shorter wavelengths) required for most applications. Versatile alternative structures have been based on the so-called 'woodpile' periodic arrangements of semiconductor rods, in which each rod may have a rectangular cross section with dimensions of order 1 μm and a length that is much larger. Such an arrangement using rods of polycrystalline silicon (dielectric constant ~13) on a Si substrate is illustrated in figure 1.10. In this structure the spatial alignments and separations between rods constitute an effective face-centred tetragonal lattice symmetry and the stop band corresponds to the 10–14.4 μm range of wavelengths. Another PBG structure that has been investigated (see [41]) is the 'inverse opal' arrangement. These are formed by utilizing the property of microscopic spheres (e.g., of silica, SiO_2) to self-assemble into an fcc lattice from a colloidal solution. The structure can then be inverted by filling the voids between spheres with a high-dielectric material and finally dissolving away the spheres.

As well as the intense activity mentioned above with the focus on 3D PBG materials, there have also been advances in developing 2D structures [41]. In particular, there have been studies of structures with artificial 2D periodicity, including cases where the dielectric functions are dispersive, giving rise to plasmons, phonons and polaritons, for example. We will discuss some of these 2D cases in the later chapters.

References

[1] Kittel C 2004 *Introduction to Solid State Physics* 8th edn (New York: Wiley)
[2] Ashcroft N W and Mermin N D 1976 *Solid State Physics* (New York: Saunders College)
[3] Grosso G and Parravicini G P 2013 *Solid State Physics* 2nd edn (Amsterdam: Academic)
[4] Cottam M G and Tilley D R 2005 *Introduction to Surface and Superlattice Excitations* 2nd edn (Bristol: IOP)
[5] Bloch F 1928 *Z. Phys.* **52** 555
[6] Novoselov K S, Geim A K, Morozov S V, Jiang D, Katsnelson M I, Grigorieva I V, Dubonos S V and Firsov A A 2005 *Nature* **438** 197

[7] Castro Neto A H, Guinea F, Peres N M R, Novosolov K S and Geim A K 2009 *Rev. Mod. Phys.* **81** 109
[8] Nénert G, Ritter C, Isobe M, Isnard O, Vasiliev A N and Ueda Y 2009 *Phys. Rev.* B **80** 024402
[9] Yariv A 1989 *Quantum Electronics* 3rd edn (New York: Wiley)
[10] Butcher P N and Cotter D 1990 *The Elements of Nonlinear Optics* (Cambridge: Cambridge University Press)
[11] Mills D L 1998 *Nonlinear Optics* 2nd edn (Berlin: Springer)
[12] Gurevich A G and Melkov G A 1996 *Magnetization Oscillations and Waves* (Boca Raton, FL: CRC)
[13] Stancil D D and Prabhakar A 2009 *Spin Waves: Theory and Application* (Heidelberg: Springer)
[14] Jackson J D 1999 *Classical Electrodynamics* 3rd edn (New York: Wiley)
[15] Griffiths D J 2012 *Introduction to Electrodynamics* 4th edn (Boston, MA: Addison-Wesley)
[16] Stegeman G I, Seaton C T, Hetherington W M, Boardman A D and Egan P 1986 *Electromagnetic Surface Excitations* ed R F Wallis and G I Stegeman (Berlin: Springer) p 261
[17] Wendler L 1986 *Phys. Stat. Solidi* B **135** 759
[18] Weisbuch B and Vinter B 1991 *Quantum Semiconductor Structures* (Boston, MA: Academic)
[19] Vollath D 2008 *Nanomaterials* (Weinheim: Wiley)
[20] Esaki L and Tsu R 1970 *IBM J. Dev.* **14** 61
[21] MacDonald A H 1987 *Interfaces, Quantum Wells, and Superlattices* ed C R Leavens and R Taylor (New York: Plenum) p 347
[22] Albuquerque E L and Cottam M G 2003 *Phys. Rep.* **376** 225
[23] Yablonovich E 1987 *Phys. Rev. Lett.* **58** 2059
[24] John S 1987 *Phys. Rev. Lett.* **58** 2486
[25] Mitin V V, Kochelap V A and Stroscio M A 2008 *Introduction to Nanoelectronics: Science, Nanotechnology, Engineering, and Applications* (Cambridge: Cambridge University Press)
[26] Aliofkhazraei M and Ali N 2012 *Two-Dimensional Nanostructures* (Boca Raton, FL: CRC)
[27] Cottam M G and Lockwood D J 1986 *Light Scattering in Magnetic Solids* (New York: Wiley)
[28] Cardona M and Güntherodt G (ed) 1989 *Light Scattering in Solids* vol 5 (Berlin: Springer)
[29] Dutcher J 1995 *Linear and Nonlinear Spin Waves in Magnetic Films and Superlattices* ed M G Cottam (Singapore: World Scientific) p 287
[30] Hillebrands B and Ounadjela K (ed) 2003 *Spin Dynamics in Confined Magnetic Structures* vol 2 (Berlin: Springer)
[31] Woodruff D P and Delchar T A 1986 *Modern Techniques of Surface Science* (Cambridge: Cambridge University Press)
[32] Feldman L C and Mayer J W 1986 *Fundamentals of Surface and Thin Film Analysis* (Amsterdam: North-Holland)
[33] Lehwald S, Szeftel J, Ibach H, Rahman T S and Mills D L 1983 *Phys. Rev. Lett.* **50** 518
[34] Hopster H 1994 *Ultrathin Magnetic Structures* vol 1 ed J A C Bland and B Heinrich (Berlin: Springer)
[35] Schreyer A, Schmitte T, Siebrecht R, Bödeker P, Zabel H, Lee S H, Erwin R W, Majkrzak C F, Kwo J and Hong M 2000 *J. Appl. Phys.* **87** 5443
[36] Brusdeylins G, Doak R B and Toennies J P 1981 *Phys. Rev. Lett.* **46** 437
[37] The Object Oriented MicroMagnetic Framework (OOMMF) project at ITL/NIST http://math.nist.gov/oommf

[38] Bransden B H and Joachain C J 2000 *Quantum Mechanics* 2nd edn (Englewood Cliffs, NJ: Prentice-Hall)
[39] Landau L D and Lifshitz E M 1980 *Statistical Physics* (Oxford: Pergamon)
[40] Cottam M G and Maradudin A A 1984 *Surface Excitations* ed V M Agranovich and R Loudon (Amsterdam: North-Holland) p 1
[41] Joannopoulos J D, Johnson S G, Winn J N and Meade R D 2008 *Photonic Crystals: Molding the Flow of Light* 2nd edn (Princeton, NJ: Princeton University Press)
[42] Rytov S M 1956 *Sov. Phys. Acoust.* **2** 68
[43] Yariv A and Yeh P 1984 *Optical Waves in Crystals* (New York: Wiley)
[44] Yablonovitch E, Gmitter T J and Leung K M 1991 *Phys. Rev. Lett.* **67** 2295
[45] Lin S Y, Fleming J G, Hetherington D L, Smith B K, Biswas R, Ho K M, Sigalas M M, Zubrzycki W, Kurtz S R and Bur J 1998 *Nature* **394** 251